RSC Sustainability

ROYAL SOCIETY OF CHEMISTRY

PAPER

View Article Online
View Journal | View Issue

Cite this: *RSC Sustainability*, 2024, **2**, 961

Recycling hazardous and energy-demanding piezoelectric ceramics using an oxide–halide perovskite upside-down composite method†

Sivagnana Sundaram Anandakrishnan, Mohadeseh Tabeshfar, Mikko Nelo, Jani Peräntie, Heli Jantunen, Jari Juuti and Yang Bai *

Piezoelectric ceramics are widely employed in electromechanical coupling components such as sensors, actuators, and transducers owing to their excellent performance, cost-effectiveness, versatile shapes and configurations, and generous chemical/functional tuneability. However, most piezoceramics contain a significant amount of the hazardous and toxic element Pb, which is considered unsustainable. Although more environmentally friendly Pb-free counterparts have been developed, production of both Pb-containing and Pb-free piezoceramics still demands high energy consumption. On the other hand, retired and rejected piezoceramics are not properly recycled, leaving a large ecological footprint for the piezoelectric industry. Thus, there is a need for proper recycling methods which give wasted piezoceramics a second life at only a marginal energy cost, so that the energy and environmental footprints are minimized before the piezoceramics are permanently disposed of. This work demonstrates the fabrication and use of oxide–halide perovskite composites to recycle piezoceramics. The composites consist of oxide perovskite piezoceramic particles as the fillers that mimic crushed/recycled piezoceramics and an organometal halide perovskite, PTMA–$CdCl_3$ (PTMA is $C_6H_5N(CH_3)_3$), as the matrix/binder. The composites consume only about 1% of the energy budget required for making new equivalent piezoceramics whilst retaining comparable capabilities for sensing applications. The results suggest that such a recycling method is applicable to a broad range of piezoceramics, providing an incentive to possibly extend the method for simultaneously recycling other oxide and halide perovskite materials and components in the future.

Received 28th September 2023
Accepted 4th March 2024

DOI: 10.1039/d3su00348e

rsc.li/rscsus

Sustainability spotlight

Piezoelectric materials are essential for modern electronics, devices and equipment but their manufacturing suffers from high energy consumption and hazardous source materials. For example, they need to be treated at ultrahigh temperatures and many products contain toxic Pb. Piezoelectric materials and products are not properly recycled nowadays, leading to a heavy carbon footprint for this polluting yet important industrial sector. In this work, we demonstrate a reliable method for recycling these energy-demanding and non-environmentally friendly materials that is transferrable to many compounds. Moreover, our method gives a second life to the recycled materials in the smart sensing and energy harvesting domains, which helps to eliminate or postpone permanent disposal of existing hazardous elements. Therefore, our work contributes to the UN sustainable development goals of affordable and clean energy (SDG 7), sustainable cities and communities (SDG 11), responsible consumption and production (SDG 12), and climate action (SDG 13).

1. Introduction

Piezoelectric materials benefit from their capability of converting a mechanical input in the form of stress or strain to an electrical potential, and *vice versa*. Such a versatile electromechanical coupling behavior has made piezoelectrics a forefront of electronics research since their discovery in 1880.[1] Essential applications of piezoelectric components can be found in devices including impact/touch sensors, accelerometers, gyroscopes, ultrasonic transducers, SAW (surface acoustic wave) devices, micro-mass sensors, transformers, high-precision actuators, micromotors, and energy harvesters.[2,3]

Among piezoelectric materials, bulk piezoceramics based on the oxide perovskite structure offer many industrial and economic benefits. For instance, there is a broad range of selections of compositions for different working conditions and functional requirements. Those compositions are highly tunable to achieve desired properties, and the materials can be fabricated into complex shapes *via* cost-effective processes for various device configurations.[1]

University of Oulu, Microelectronics Research Unit, Faculty of Information Technology and Electrical Engineering, FI-90570 Oulu, Finland. E-mail: yang.bai@oulu.fi

† Electronic supplementary information (ESI) available. See DOI: https://doi.org/10.1039/d3su00348e

However, a major concern regarding piezoceramics is the extensive use of the hazardous and toxic element Pb. This is not compliant with the EU's legislation, RoHS (Restriction of Hazardous Substances in Electrical and Electronic Equipment), which intends to ban the use of hazardous elements in electronic devices,[4,5] whereas the widely used piezoceramic composition, the PZT ($Pb(Zr,Ti)O_3$) family, contains a significant amount of Pb (up to 68 wt%). Environmentally friendly Pb-free piezoceramics have been developed to tackle this issue.[6] Some Pb-free alternatives are able to perform similarly to their Pb-based counterparts.[6,7]

Regardless of being environmentally friendly, manufacturing of Pb-free piezoceramics, as is the case also for Pb-based piezoceramics and most other ceramics in general, involves at least two high-temperature treatment steps: (i) calcination (usually >600 °C) for formation of desired phases, and (ii) sintering (usually >1000 °C) for necessary material densification and grain growth.[1] The sintering is particularly important because most signature functionalities of piezoceramics, such as excellent piezoelectric coefficients and strong electromechanical coupling, are obtained only after this step.

The need for high-temperature treatments inevitably leads to high energy consumption, making all industrial sectors which deploy piezoelectric components energy intensive and unsustainable. In addition, the high-temperature densification procedure causes unpredictable shrinkage as large as 15–25% and unfavored chemical diffusion when co-sintered with other materials, both of which significantly degrade the compatibility of piezoceramics for integration with other components.[8]

One method to reduce the energy footprint of piezoceramic manufacturing is to properly recycle retired or broken piezoelectric components after use as well as the low-quality ones that have already been rejected during fabrication. Ideally, the recycled materials should also be given a second life at service to the best possible extent before they are permanently disposed of. A prerequisite here is that the recycling procedure consumes only a marginal amount of energy compared to that needed for making correspondingly new materials. Meanwhile, the materials made *via* recycling should obtain comparable properties to those of newly sintered piezoceramics. Otherwise, the energy benefit provided by recycling will be outweighed by the better performance of newly made materials.

Among possible methods that can be utilized for recycling piezoceramics,[7,9] the ultralow-temperature densification route is considered viable due to low energy consumption and simple fabrication procedures.[10–12] In this method, a small amount of liquid acts as a transport phase during densification of a functional filler phase under pressure, with or without mildly elevated temperature (<350 °C). In particular, the transport phase coats the filler particles to form a core–shell microstructure,[8] and upon applying high pressure, the transport phase redistributes itself due to surface tension and capillary action. Dissolution of the filler particles into the transport phase occurs at contacting points which experience a very high, GPa-level local pressure. The dissolved filler phase then, due to evaporation of the transport phase at mild temperature or at room temperature though with a slower pace, reprecipitates at sites away from the contacted edges due to a favorable concentration gradient which drives densification and grain growth.[13]

The ultralow-temperature densification method has shown promise using dielectric ceramic particles as the filler phase. For instance, the first truly room-temperature densified ceramic has been reported where Li_2MoO_4 (LMO) particles are used as the filler phase with deionized water as the transport phase, which are then shaped and densified under 130–150 MPa.[10,11] The subsequently obtained dielectric properties are measured to be better than those of the LMO ceramics conventionally sintered at 540 °C. The advantage here is that the functional phase, LMO, is soluble in water. The LMO–water solution also acts as a functional binder and precipitates in the intergranular areas between the filler particles through redistribution and evaporation of the solution under pressure. This has eased transportation of the functional filler phase to a large extent in the form of a transport solution and hence, after being shaped under high pressure, better functionality is achieved. The resultant material is a ceramic–ceramic composite with much higher filler volume fraction compared to the case for conventional composites, and it is thus termed an 'upside-down' composite. Using LMO as the binder phase, TiO_2-based,[12] $SrTiO_3$-based,[14] and $(Ba_{0.55}Sr_{0.45})TiO_3$-based[15] dielectric upside-down composites have been successfully made.

Recently, piezoelectric upside-down composites have also been made using PZT as the filler.[16] Instead of LMO–aqueous solution, an organotitanate precursor gel has also been applied as the binder.[17] Under a pressure of 250 MPa and at 300 °C, the precursor gel forms amorphous TiO_2 (am-TiO_2) in the intergranular areas of the PZT particles and thus an upside-down PZT–(am-TiO_2) composite is obtained in addition to the PZT–LMO composite.

It is worth noting that the PZT fillers used in the above-mentioned composites are made by crushing high-temperature sintered ceramics. Although the method itself does not save energy in a new fabrication round, it adds merits to a possible recycling procedure because mechanically and/or electrically broken piezoceramic components, which need to be reshaped, are naturally appropriate sources of the filler materials. Moreover, although the PZT–LMO and PZT–(am-TiO_2) composites perform worse than the PZT ceramics in terms of generic piezoelectric response, they are particularly competitive regarding the piezoelectric voltage coefficient (g)[16,17] which is an indicator for potential sensitivity of piezoelectric sensors made from the same material. The possible recycling is then highly likely to succeed in making sensors from a wide range of recycled piezoceramics. Therefore, this work reports the recycling of Pb-based and Pb-free piezoceramics using the upside-down composite fabrication method with an organometal halide perovskite compound, PTMA–$CdCl_3$ where PTMA is $C_6H_5N(CH_3)_3$ (ref. 9 and 18), as the binder phase.

The motivation here is attributed to the compound's capability of dissolving in an organic solvent (advantageous over LMO to reduce hygroscopicity) and its subsequent recrystallization at closer to room temperature (advantageous over TiO_2 to eliminate the need for further elevated temperature). In this

work, four types of filler materials are chosen, including two Pb-free piezoceramics, $BaTiO_3$-based[19] and (K,Na)NbO_3-based,[20] and two Pb-based ones, soft-type[21] and hard-type[22] PZT, respectively. The four chosen compositions tend to represent a wide range of piezoceramics used in different categories of applications under various working conditions and with distinctive functional requirements. The results obtained from these four types of upside-down composites are compared to their pristine ceramic counterparts to evaluate the extent of gain or degradation in functional properties.

2. Materials and methods

2.1. Fabrication of piezoceramic pellets and fillers

Table 1 summarizes the materials fabricated in this work, including information on filler compositions, binder volume fractions (where applicable), and densities. Four types of oxide perovskite structured piezoceramics were fabricated *via* the solid-state route. The two Pb-free ceramic powders were synthesized. Reactants of $BaCO_3$ (99%, Alfa Aesar, Germany) and TiO_2 (99.9%, Aldrich Chemistry, Canada) for $BaTiO_3$ (BT), and K_2CO_3 (99%, J.T. Baker, Holland), Na_2CO_3 (99%, Sigma-Aldrich, Germany), $BaCO_3$ (99.98%, Sigma-Aldrich, USA), Nb_2O_5 (99.9%, Aldrich, China) and NiO (99.999%, Aldrich Chemistry, USA) for $(K_{0.52}Na_{0.38}Ba_{0.03})(Nb_{0.985}Ni_{0.015})O_{2.9575}$ (KNBNNO) were first weighed according to stoichiometry.

Ball-milling was then performed with ZrO_2 beads (for BT) or without beads (for KNBNNO as the use of beads during mixing of raw powders caused substantial stoichiometric loss of alkali carbonates) in ethanol for 6 hours. The dried mixture was subjected to calcination at 1100 °C (BT) or 750 °C (KNBNNO) for 4 hours. K_2CO_3, Na_2CO_3 and NiO were stored at 220 °C prior to weighing owing to their hygroscopicity.[23]

The two Pb-based ceramic powders, H-PZT (APC-841, a hard-type PZT) and S-PZT (PZ29, a soft-type PZT), were purchased from American Piezo International (APC) Ltd. (USA) and Meggitt A/S (Denmark), respectively. To obtain a suitable particle size distribution, a ball milling procedure was performed for the as-purchased powders with ZrO_2 beads in ethanol for 12 hours. The same procedure was also performed for the calcined Pb-free powders. After drying, each milled powder was sieved through a 200 μm mesh and was then shaped into green bodies with diameter of 10 mm for BT, KNBNNO and H-PZT, 13 mm for S-PZT, and 14.5 mm for all ceramic powders under uniaxial pressure of approximately 90–110 MPa using polyvinyl alcohol (PVA) as the binder. The binder was subsequently burnt off at 550 °C for 10 hours and the green bodies were finally sintered at 1450 °C for 4 hours (BT, on a Pt substrate), at 1150 °C for 2 hours (KNBNNO, on a Pt substrate), at 1100 °C for 4 hours (H-PZT, in an alumina crucible), and at 1200 °C for 2 hours (S-PZT, in an alumina crucible), respectively. Note that the KNBNNO samples were covered under an alumina crucible during sintering to help suppress possible evaporation of the alkali elements.[23] Also, powder beds were made for the H-PZT and S-PZT using the same corresponding powders and the samples were covered under an alumina crucible to help prevent possible loss of Pb during the high-temperature sintering process.[1] Dimensions of the four types of sintered pellets are shown in Table S1 in the ESI.†

Smaller ceramic pellets were structurally and electrically characterized, whereas the larger pellets shaped with the 14.5 mm die were crushed in a mortar using a pestle. The crushed ceramics were sieved through a series of meshes of 425 μm, 180 μm, and 63 μm, consecutively. Particles in sizes between 63 and 180 μm, which mimicked filler materials recycled from worn-out devices, were collected for the following upside-down composite fabrication.

2.2. Synthesis of PTMA–$CdCl_3$

The starting reactants of PTMA–Cl (≥98%, Sigma-Aldrich, USA) and $CdCl_2$ (99.99%, Sigma-Aldrich, USA) were weighed stoichiometrically. A mixed solution of acetonitrile and deionized water (volume ratio of 3 : 2) was used to dissolve the reactants in a concentration of 13.3 w/v% and then the solution containing

Table 1 Summary of compositions and densities of the piezoceramics and upside-down composites fabricated in this work

Sample ID	Form of material	Filler composition	Binder volume fraction (%)	Measured density (g cm^{-3})	Theoretical density (g cm^{-3})	Relative density (%)
BT-P	$Ba(Zr_xTi_{1-x})O_3$ ceramic pellet	—	—	~5.44	5.90 ± 0.06	92.2 ± 1.0
KNBNNO-P	$(K_{0.52}Na_{0.38}Ba_{0.03})(Nb_{0.985}Ni_{0.015})O_{2.9575}$ ceramic pellet	—	—	~4.34	4.53 ± 0.07	95.8 ± 1.5
H-PZT-P	Hard-type PZT ceramic pellet	—	—	~7.58	7.86 ± 0.14	96.5 ± 1.7
S-PZT-P	Soft-type PZT ceramic pellet	—	—	~7.17	7.54 ± 0.10	95.1 ± 1.3
BT-C	Composite	$Ba(Zr_xTi_{1-x})O_3$	~14.7	4.52 ± 0.12	~5.30	85.4 ± 2.2
KNBNNO-C	Composite	$(K_{0.52}Na_{0.38}Ba_{0.03})(Nb_{0.985}Ni_{0.015})O_{2.9575}$	~11.7	3.59 ± 0.03	~4.21	85.2 ± 0.6
H-PZT-C	Composite	Commercial hard-type PZT	~18.7	5.93 ± 0.05	~6.72	88.1 ± 0.8
S-PZT-C	Composite	Commercial soft-type PZT	~18.1	6.05 ± 0.05	~6.50	93.0 ± 0.8

$C_6H_5N(CH_3)_3^+$, Cd^{2+}, and Cl^+ was stirred for 24 hours.[18] After passing through a 0.2 μm PTFE (polytetrafluoroethylene) filter, cm-sized PTMA–$CdCl_3$ crystals were grown *via* slow precipitation statically in 3–4 weeks.

2.3. Fabrication of upside-down composites

Using crushed and particle size-controlled (63–180 μm) ceramics as the filler and PTMA–$CdCl_3$ as the binder, four types of upside-down composites were made. 60 w/v% of ceramic filler particles were added in a 0.6 v/w% PTMA–$CdCl_3$ acetonitrile–deionized water solution. The suspension was kept being stir-mixed whilst evaporating the solvents on a hot plate. Filler particles coated with PTMA–$CdCl_3$ were obtained after the suspension was dried. Such a coating procedure followed the same mechanism as is reported in the literature.[15] The coated filler particles were then mixed with 5 wt% crushed PTMA–$CdCl_3$ crystals in a mortar with a pestle. During mixing, 3–4 drops of saturated PTMA–$CdCl_3$ solution (prepared in Section 2.2) was also added to each gram of the filler material as the transport phase during shaping. The obtained mixture was then uniaxially hot-pressed in a cylindrical steel mold of 10 mm diameter under 250 MPa and at 150 °C for 30 minutes. Before releasing the pressure and being removed from the mold, the sample was cooled down to 50 °C. The amount of filler used to prepare each upside-down composite sample and dimensions of the composite samples are listed in Table S1.†

2.4. Structural and electrical characterization

The density of the samples was measured using either Archimedes' method in ambient air and deionized water or the dimensional method (weight/volume). XRD (X-ray diffractometry) was used to analyze phases of crushed ceramics using a diffractometer (SmartLab 9 kW, Rigaku, Japan) under Co $K\alpha_1$ radiation ($\lambda = 1.7889$ Å) at a scanning rate of 4° min^{-1} for 2θ. Lattice parameters were determined using the Rietveld refinement method in PDXL2 software. Elemental analysis was carried out on the carbon-coated surface of ceramic pellets using an electron-probe microanalyzer (EPMA) (JXA-8530F Plus, JEOL, Japan) with 15 kV acceleration voltage, 15 nA probe current, and 1–5 μm beam spot size. Nominal chemical formulae of the ceramics were calculated from the EPMA results. Using the unit cell volume (V) calculated from XRD results and theoretical molecular weight (A) calculated from EPMA results, the theoretical density (ρ_f) of each filler material was calculated based on eqn (1), where N is Avogadro's number and n is number of atoms per unit cell. Eqn (2) calculates the binder volume fraction (ϕ_b) in the composite, where m_f is the mass fraction of the filler (0.95 for all samples) and ρ_b is the theoretical density of PTMA–$CdCl_3$ (~1.80 g cm^{-3}, provided by single crystal XRD measurement in previous work[18]). Eqn (3) determines the theoretical density of the composite (ρ_c) with volume fractions of the filler (ϕ_f) and ϕ_b.

$$\rho_f = \frac{nA}{vN} \quad (1)$$

$$\phi_b = 1 - \frac{\rho_b}{\rho_f\left(\frac{1}{m_f} - 1\right) + \rho_b} \quad (2)$$

$$\rho_c = \rho_b\phi_b + \rho_f\phi_f \quad (3)$$

The cross-sectional surface of the composite samples was polished in a vacuum under a cooling cross-section ion polisher (JEOL IB-19520CCP, Japan) with a stainless-steel source. The polished, carbon-coated surface was characterized under a field-emission scanning electron microscope (FESEM, ULTRA Plus, Carl Zeiss SMT AG, Germany) equipped with an energy dispersive X-ray spectroscopy (EDS) system under an acceleration voltage of 15 kV.

The ceramic pellets were polished down to 0.95–1.05 mm thick from both surfaces on a P1200 abrasive paper. Polished H-PZT and KNBNNO pellets were painted with an Ag-epoxy paste (H20E-4GM, Epoxy Technology, USA) which was cured at 150 °C for 30 minutes as the electrode. Polished S-PZT and BT pellets were screen-printed with an Ag conductive paste (735825, Sigma-Aldrich Co., South Korea) which was cured at 120 °C for 30 minutes. Another Ag conductor paste (5065, Dupont, UK) was painted on the composite samples and was cured at 130 °C for 10 minutes as the electrode.

Dielectric properties were measured at room temperature in the dark with an LCR meter (E4980AL, Keysight Technologies, USA). Poling was performed in the dark, in a silicone oil bath, and at room temperature for a period of 10 minutes. The poling electric fields for both ceramics and composites were 3 kV mm^{-1}, 4 kV mm^{-1}, 6 kV mm^{-1}, and 3 kV mm^{-1} for BT, KNBNNO, H-PZT, and S-PZT, respectively. The poled samples were electrically shorted for 24 hours, and their respective longitudinal piezoelectric charge coefficient (d_{33}) was subsequently measured with a d_{33} meter (YE2730A, APC International Ltd., USA) under 0.25 N alternating force at 110 Hz.[24]

3. Results and discussion

3.1. Phases and microstructure

Data associated with this work are openly available.[25]

The rationale for choosing these four piezoceramic compositions as the fillers was that they represent a broad range of material features and piezoelectric applications. BT-based compositions are popular Pb-free options showing moderate to very high piezoelectric response with relatively low Curie temperature compared to other piezoelectric counterparts.[6] Their structural and electrical properties have been well understood in a large number of previous studies.[26,27] They are also widely used in MLCCs (multilayer ceramic capacitors), which are an essential component with each electronic device containing hundreds or thousands of units.[28] Therefore, BT was an ideal fundamental composition to study in this work, assuming the large MLCC market and other BT-based piezoelectric components to be potential resources for future recycling.

The KNN ($(K,Na)NbO_3$) based compositions are another popular family of Pb-free piezoelectrics featuring high Curie

temperature and impressive piezoelectric response.[6] However, since pure KNN is hygroscopic and thus is unstable in ambient air with moisture being present, this work studied the KNBNNO as a representative KNN-based filler. It has been proven in previous research that minor doping of Ba and Ni in KNN could result in a much better stability of the fabricated ceramic samples working in a wet environment.[29] This makes the KNBNNO filler suitable for the organometal halide perovskite coating procedure in an aqueous solution carried out in this work. KNBNNO's chemical formula used in this work was selected for the optimum piezoelectric response by screening data reported in previous works.[20]

Both the H-PZT and S-PZT are from the PZT family, but they exhibit distinctive properties. H-PZT is a hard-type PZT featuring high Curie temperature, high mechanical strength, low dielectric loss, and large coercive field. They are often used in actuators such as piezoelectric motors and vibration control units.[1]

S-PZT is a soft-type PZT featuring very high piezoelectric response, but lower Curie temperature, higher dielectric loss, and smaller coercive field compared to H-PZT. Their excellent piezoelectricity is usually employed in high-sensitivity sensors and energy harvesters.[3,30–32] In addition, studying how to recycle these two Pb-based compounds has an extra benefit for solving the environmental issues as presented in the introduction.

Fig. S1 in the ESI† shows the pictures of sintered ceramic pellets and their corresponding upside-down composites fabricated in this study. The dimensions of the ceramic and composite samples were made comparable to each other for a fair evaluation of the microstructural and functional changes from ceramics to composites. XRD reflections of the four ceramic fillers are shown in Fig. 1 marked with corresponding perovskite (ò) and secondary (#) phases. The Rietveld refinement results are shown in Fig. S2–S5 and Tables S2–S9 in the ESI† using PDF numbers of 00-066-0857, 01-087-7260, 00-067-0380, and 01-070-0638 as the major phase references and 04-005-5869, 04-006-0584, and 04-014-5162 as the secondary phase references. Accurate chemical compositions of all the fillers calculated from the EPMA results are displayed in Table S10 in the ESI.† Fig. 2 demonstrates the microstructure of the BT composite (BT-C) by FESEM micrograph and EDS maps. Fig. S6–S8† display the microstructure of other composite samples, *i.e.*, KNBNNO-C, H-PZT-C, and S-PZT-C, respectively.

From Fig. S2–S5,† good fits are obtained for all fillers with the parameter R_p, which quantifies the exactness of the fit to the observed XRD reflections, remaining at low values of <10%. Expected oxide perovskite phases were properly formed in all the ceramic samples with space groups of *P*4*mm* (tetragonal perovskite phase) for H-PZT and S-PZT, and *Amm*2 (orthorhombic perovskite phase) for BT and KNBNNO. Although BT was expected to have a tetragonal perovskite phase as is commonly observed,[27] Zr ingress (≈3 mol%), which might be introduced with impurities of the starting reactants or during the milling procedure, caused a phase shift from tetragonal to orthorhombic that is consistent with the literature.[33] The Zr ingress is also evident in the EDS images of Fig. 2. A secondary phase (Fig. 1a) was defined as Ba_2ZrO_4 (space group: 139: *I*4/*mmm* and tetragonal crystal structure) with reflections at 2θ of 31.82°, 34.07°, 45.61°, and 58.14°. A reflection at 2θ of 33.40° could not be identified, possibly due to minor impurities present in the starting reactants.

In Fig. 1b, the lattice parameters of the perovskite phase for KNBNNO agreed with those in the literature.[34] In addition, a secondary phase was formed with evidence of minor reflections between 29° and 42°. They matched a tungsten bronze phase with a chemical formula of $Ba_3Nb_{4.67}Ni_{0.33}O_{15}$ (space group: 100: *P*4*bm* and tetragonal crystal structure) which is also typically seen in the literature.[20] According to Fig. 1c and d, both the sintered H-PZT and S-PZT ceramics formed expected perovskite phases which were identical to those existing in the as-purchased powders. However, the H-PZT had some reflections attributed to secondary or unknown phases at various 2θ across the measurement range. This might be because of possible Pb loss during sintering which caused an uneven distribution of dopants. Evidence could be found in the EDS maps for the hard-PZT composite (H-PZT-C) in which Sb and Mn were seen to be inhomogeneously spread across the filler particles, as shown in Fig. S7.† As expected, the secondary phase was matched to $Pb(Zr_{0.5}Ti_{0.5})O_3$ (space group: 227: $Fd\bar{3}m$, choice-2 and cubic crystal structure). Similarly, the S-PZT had an unidentified reflection at 2θ of 49.7° which could be assigned to the segregated Sr detected in the fillers of the soft-PZT composite (S-PZT-C), as shown in Fig. S8.†

According to subsequently calculated data shown in Table 1, all the ceramic pellets achieved relative densities of 91–97%, indicating good microstructural quality of the sintered ceramic fillers.

The good filler quality, together with the proper selection of the binder, consequently induced high-quality upside-down composites. As demonstrated in Fig. 2, a high packing density between the BT filler and PTMA–$CdCl_3$ binder particles can be observed. Referring to the term upside-down composite, the FESEM micrograph and EDS maps clearly visualized the high volume-fraction of the BT filler. Meanwhile, no major microstructural defects, such as voids, pores, or cracks, were noticed at the boundaries between BT and PTMA–$CdCl_3$ particles. Similar situations shown in Fig. S6–S8† concluded a successful fabrication of the upside-down composites between oxide and halide perovskites in this work with a similar microstructure that has been reported in previous works.[15,16] EDS maps for all the composites indicated that constitutive elements of the fillers and those of the binder were seen only in their respective particles. This implies that no reaction happened between the filler and binder, likely due to the process combining a lower fabrication temperature and a pressure-assisted densification procedure which did not provide enough activation energy for cross reaction, as opposed to the case for high-temperature sintering.

3.2. Dielectric properties

Fig. 3 shows the frequency-dependent dielectric properties of samples BT-P (ceramic) and BT-C (composite) in the frequency range of 20 Hz to 100 kHz. The frequency dependent dielectric

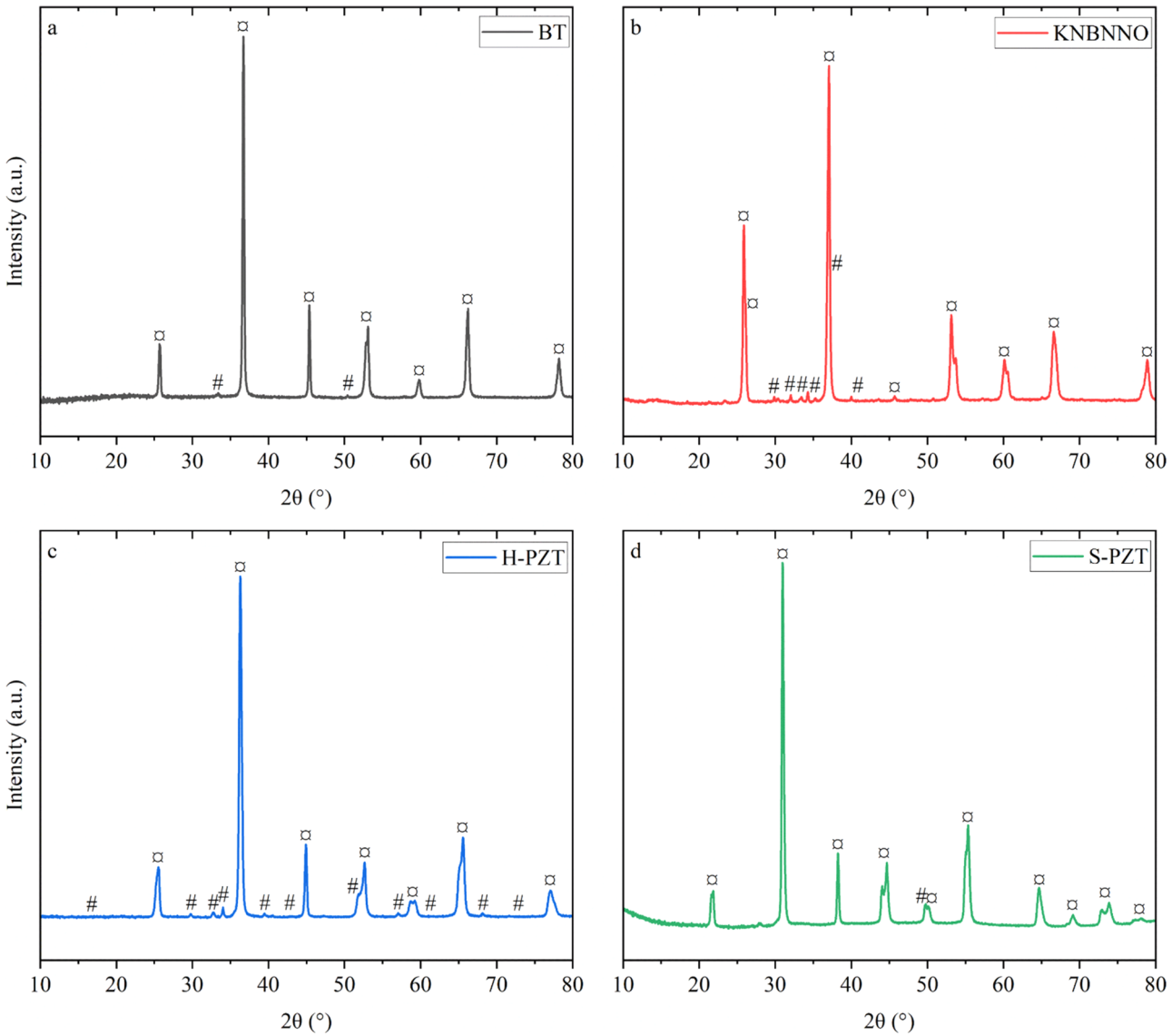

Fig. 1 XRD reflections of piezoceramic fillers: (a) BT, (b) KNBNNO, (c) H-PZT, and (d) S-PZT. Major perovskite phases are marked with 'ò' and secondary phases are marked with '#'.

properties for the KNBNNO, H-PZT and S-PZT ceramic and composite samples in the same frequency range are shown in Fig. S9–S11 in the ESI.†

The relative permittivity (ε_r) and dielectric loss (tan(δ)) for both the unpoled and poled states are provided in the figures. The distinctive values of unpoled and poled permittivity and dielectric loss indicated an effective poling procedure for all the ceramic and composite samples. From the figures, it is seen that the composite samples generally exhibited a decreasing trend of permittivity and dielectric loss with the increase of frequency,

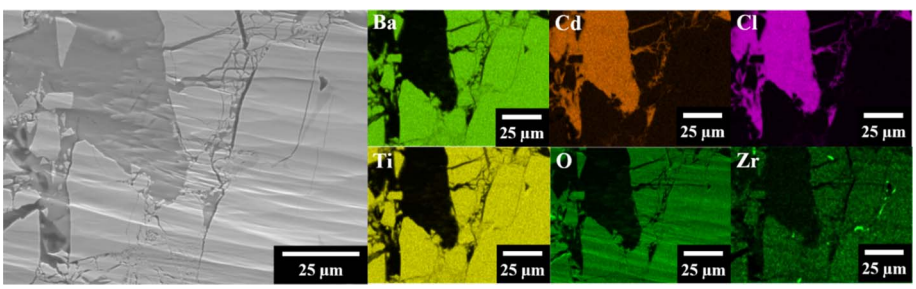

Fig. 2 FESEM micrograph and EDS maps of upside-down composite sample BT-C.

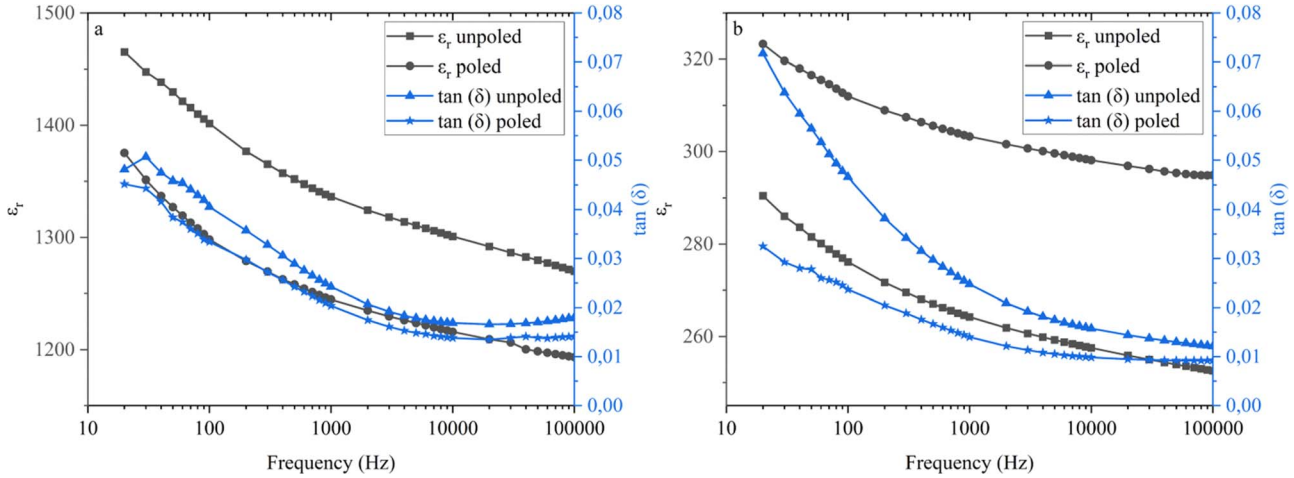

Fig. 3 Dependence of relative permittivity (ε_r) and dielectric loss (tan(δ)) on frequency for unpoled and poled (a) BT-P and (b) BT-C measured at room temperature in the dark.

whereas some ceramic samples such as KNBNNO-P and S-PZT-P tended to be more sensitive to frequency change. The behavior of frequency dependence was affected by different resonant frequencies of dipoles and ferroelectric domains.[35] All the composite samples had poled permittivity values greater than their respective unpoled permittivity values possibly owing to a ferroelastic contribution from the PTMA–$CdCl_3$ binder.[18] During poling of the composites, the ferroelastic properties of the PTMA–$CdCl_3$ binder eased the domain pinning effect that would have otherwise resulted on the fillers with a non-ferroelastic binder. This type of polarization behaviour has already been observed in ferroelectric hysteresis loops conducted on upside-down composites fabricated with PTMA–$CdCl_3$ as a binder.[9]

In the ceramic samples, the trend of the unpoled and poled permittivity values was not straightforward compared to the composite samples. For instance, in the H-PZT-P and S-PZT-P ceramic samples, the unpoled permittivity values were smaller than their poled counterparts. This is attributed to the tetragonal crystal structures of their primary phases (Tables S7 and S9†). Increased permittivity after poling is often empirically observed due to the dominance of 180° domain reorientation.[36,37]

The evolution of permittivity after poling for the BT-P and KNBNNO-P ceramics was analogous with orthorhombic phases identified (Tables S3 and S5†), giving decreased permittivity values in the poled states associated with non-180° domain reorientation.

Fig. 4 compares the dielectric properties between the ceramic and composite samples in a more straightforward way by extracting unpoled relative permittivity and dielectric loss values at 1 kHz. Percentages of ε_r and tan(δ) for the composites with respect to those for the ceramic counterparts are also placed alongside. As can be seen in Fig. 4, all the ceramics achieved comparable dielectric properties to those reported in the literature correspondingly.[20,26,38,39] More information can be found in data associated with this work.[25]

As shown in Fig. 4a, the BT composite (BT-C) yielded the largest relative permittivity ($\approx$245) compared to other composites (*i.e.*, $\approx$170 for KNBNNO-C and $\approx$210 for H-PZT-C and S-PZT-C). It can also be noticed that across different compositions, the distribution of ε_r values of the composites was relatively narrow (*i.e.*, within 30–45% variation) compared to that of the ceramics (*i.e.*, as large as 50–120% variation).

The reduced and narrowly distributed permittivity in the composites was due to the interplay between the inherent contribution of permittivity from the filler to the composite and thus the 'composite effect' that occurred between a high-permittivity filler and a low-permittivity binder ($\varepsilon_r \approx 10$ for the PTMA–$CdCl_3$ crystal[18]). A larger difference between permittivity values of the filler and binder would increase the dominance of the binder in contribution to measured permittivity of the overall composite.[40–42] This phenomenon appeared due to a lack of interconnectivity between the filler particles in 0–3 composites where fillers are randomly dispersed in the binder, which is the case in this work. During the LCR measurement, the input electric field was actually applied more on the low-permittivity binder than on the high-permittivity fillers.[40,41,43]

Therefore, the largest ε_r value exhibited by BT-C among all the composites was attributed to a moderate permittivity value of the BT filler acting against its own composite effect (Fig. 3a). The composite effect could also be clearly seen when assessing the retainment of ε_r values in composites compared to those in corresponding ceramics. As shown in Fig. 4a, the percentage of ε_r values of the composites out of their ceramic counterparts was about 20% for the pairs of BT-C/BT-P, KNBNNO-C/KNBNNO-P and H-PZT-C/H-PZT-P. However, the percentage for the S-PZT-C/S-PZT-P pair was only about 10% owing to more disparate permittivity values between the S-PZT filler and the PTMA–$CdCl_3$ binder (Fig. S11a†).

It should be noted that the upside-down composites prepared in this study had filler volume fractions higher than that in conventional 0–3 dielectric and piezoelectric composites which enabled the filler's permittivity to have a more significant

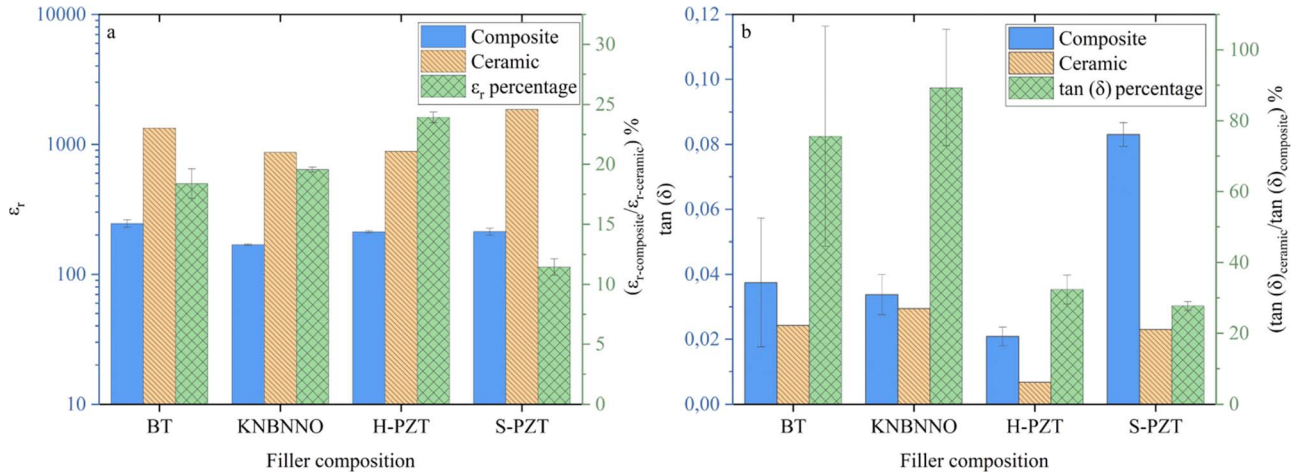

Fig. 4 (a) Relative permittivity (ε_r) and (b) dielectric loss (tan(δ)) of unpoled BT, KNBNNO, H-PZT, and S-PZT ceramic and composite samples measured at 1 kHz, and ratio of (a) the composite relative permittivity value ($\varepsilon_{r\text{-composite}}$) to the corresponding ceramic relative permittivity value ($\varepsilon_{r\text{-ceramic}}$) shown as a percentage (($\varepsilon_{r\text{-composite}}/\varepsilon_{r\text{-ceramic}}$)%) and (b) the ceramic dielectric loss value ($\tan(\delta)_{ceramic}$) to the corresponding composite dielectric loss value ($\tan(\delta)_{composite}$) shown as a percentage (($\tan(\delta)_{ceramic}/\tan(\delta)_{composite}$)%) for the four compounds.

influence in the whole composite sample and thus the composite effect in this work was less severe compared to the cases in previous works.[44,45] This also provides an advantage of using upside-down composites over using conventional 0–3 composites for recycling.

As can be seen in Fig. 4b, tan(δ) values of the composites were in the range of 0.02–0.08 and they were higher than those of their ceramic counterparts. This was due to the same composite effect discussed above, which forced the electric field during LCR measurement to concentrate on the highly lossy PTMA–$CdCl_3$ binder (tan(δ) $\approx$ 0.25 (ref. 18)) rather than on the low-loss fillers (tan(δ) $\approx$ 0.01–0.03).

The composite effect phenomenon also explains the largest tan(δ) value of $\approx$0.08 in S-PZT-C among all the composites because of exaggerated distortion of electric field distribution between the filler and binder, as discussed above. The S-PZT-P and H-PZT-P showed the lowest level of tan(δ) values and, as a result, the ratio of the ceramic tan(δ) value to the composite tan(δ) value was significantly lower for these two compounds (Fig. 4b). However, the absolute tan(δ) values for these two types of composites were distinctive where S-PZT-C was three times more lossy (tan(δ) $\approx$ 0.08) than H-PZT-C (tan(δ) as low as 0.02). The higher loss in S-PZT-C could also be augmented by the 'soft' properties of the S-PZT filler.[46,47] The H-PZT-C implied a good retention of the 'hard' properties of its filler in the composite.

In addition to the influence caused by the difference between the filler and binder, the dielectric properties of the composites could also be affected by possible presence of microstructural voids such as intergranular pores, although no major pores were visualized in the microstructure of the fabricated upside-down composites (Fig. 2 and S6–S8†).

3.3. Piezoelectric properties and trade-off between energy consumption and performance

Fig. 5 and Table 2 compare the piezoelectric properties of the ceramic and composite samples fabricated in this work between each other as well as with relevant piezoceramics and composites selected from the literature, including frequently studied excellent compositions and their variants based on BT, $(Ba_{0.85}Ca_{0.15})(Ti_{0.9}Zr_{0.1})O_3$ (BCZT), KNN, PZT, $Pb(Mg_{(1/3)}Nb_{(2/3)})O_3$–$PbTiO_3$ (PMN–PT), and commercial PZT-5A.[16,17,32,48–58]

Fig. 5a shows the d_{33} values of the four types of ceramics and their corresponding composites studied in this work alongside the percentage of the composite d_{33} values with respect to those of their ceramic counterparts. The percentages provide information on the retainment of the piezoelectric properties of the fillers after being fabricated into upside-down composites. According to Fig. 5a, all the ceramics exhibited comparable d_{33} values to those reported in the literature.[20,26,38,39] This proves that the presence of the identified and unidentified secondary or impurity phases detected by XRD (Fig. 1) did not degrade the piezoelectric properties to a noticeable extent and thus was not considered as an issue for the upside-down composites made with these ceramic fillers.

Fig. 5a also shows the fact that variation of the ceramic and composite d_{33} values followed the same trend, *i.e.*, S-PZT-P ($\approx$510 pC N^{-1}) > BT-P ($\approx$295 pC N^{-1}) > H-PZT-P ($\approx$200 pC N^{-1}) > KNBNNO-P ($\approx$85 pC N^{-1}) for ceramics, and S-PZT-C ($\approx$100 pC N^{-1}) > BT-C ($\approx$45 pC N^{-1}) > H-PZT-C ($\approx$40 pC N^{-1}) > KNBNNO-C ($\approx$20 pC N^{-1}) for composites. This fact indicated that no net effect on piezoelectric properties was contributed by the binder. The decrease of d_{33} from the ceramics to the composites could be attributed to reasons as follows:

(1) As has been explained for dielectric properties, the electric field distribution inside the composite samples was dominated by the low-permittivity PTMA–$CdCl_3$ which was induced by the composite effect. As a result, the actual poling electric field in the composite was lower than the applied electric field,[45,59] as illustrated by eqn (4), where E_{filler} is the electric field in the filler, $E_{applied}$ is the applied electric field, R is the ratio of the average filler particle size to the filler interparticle distance, and ε_{binder} and ε_{filler} are relative permittivities of the PTMA–$CdCl_3$ and filler, respectively.

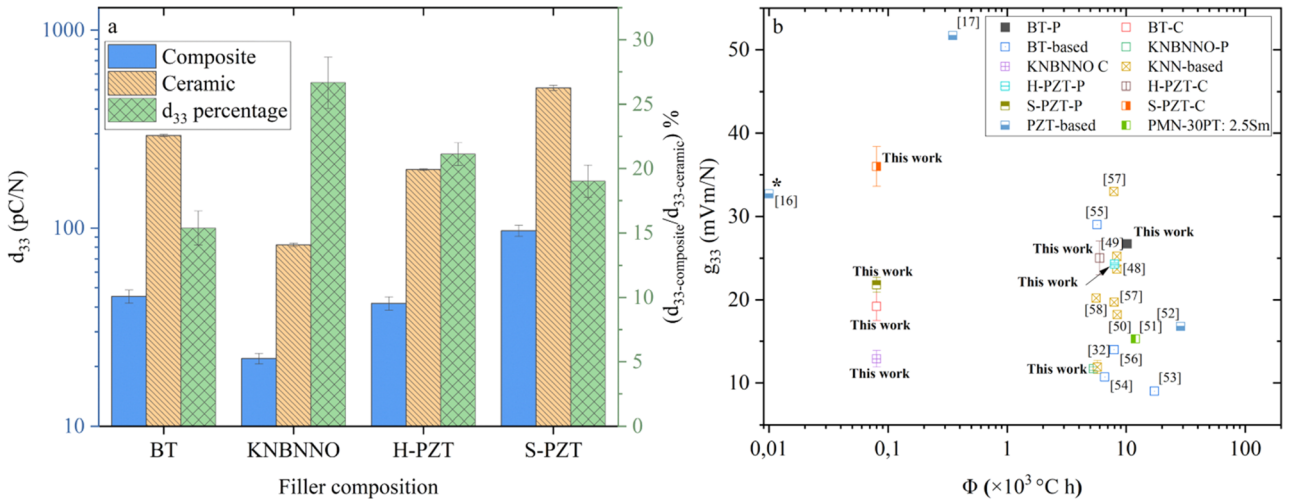

Fig. 5 (a) d_{33} of poled BT, KNBNNO, H-PZT and S-PZT ceramic and composite samples and ratio of the composite d_{33} value ($d_{33\text{-composite}}$) to the corresponding ceramic d_{33} value ($d_{33\text{-ceramic}}$) shown as a percentage (($d_{33\text{-composite}}/d_{33\text{-ceramic}}$)%); and (b) dependence of longitudinal piezoelectric voltage coefficient (g_{33}) on the energy budget of fabrication (Φ) for the ceramic and composite samples studied in this work as well as for selected high-performance counterparts reported in the literature.[16,17,32,48–58] In (b), the datapoint marked with * has an actual value of zero.

$$E_{\text{filler}} = E_{\text{applied}}\left(\frac{(1+R)\varepsilon_{\text{binder}}}{R\varepsilon_{\text{binder}} + \varepsilon_{\text{filler}}}\right) \quad (4)$$

This reason was supported by the comparison between KNBNNO-C and other composite samples where the ratio of composite d_{33} to ceramic d_{33} was the highest for KNBNNO-C because of the least disparate permittivity values between the KNBNNO filler and PTMA–$CdCl_3$ binder (Fig. S9a†) and thus the smallest influence on d_{33} by the composite effect.

(2) Lack of piezoelectricity in the PTMA–$CdCl_3$ binder[9] formed an inactive barrier between the filler particles, reduced the interconnectivity of short-range piezoelectric response, and consequently suppressed long-range piezoelectric response.

(3) As can be seen in Table 1, the composite samples had lower relative densities (85–93%) compared to their ceramic counterparts (91–97%), indicating a higher porosity in the composites. Higher porosity is a characteristic of pressure-assisted densification processes made between two elastically dissimilar materials.[15,16]

Despite inferior d_{33}, the composite samples showed piezoelectric voltage coefficient (g_{33}) values comparable to, or even larger than, those of corresponding ceramic samples, as is listed in Table 2. Variation of the g_{33} followed a similar trend to that for the d_{33} among the composite samples, as g_{33} is dependent on d_{33} and ε_r (calculated as $g_{33} = d_{33}/\varepsilon_r\varepsilon_0$ where ε_0 is permittivity in a vacuum). In this regard, S-PZT-C showed the optimum g_{33} value of $\approx$36 mV m N^{-1} as a result of its largest d_{33} and moderate permittivity among the composites. S-PZT-C also showed a larger g_{33} than S-PZT-P ($\approx$25 mV m N^{-1}). Such an increase of g_{33} benefited from the composite effect which significantly lowered the material's permittivity. A similar mechanism has also been employed by research works on porous piezoelectric materials.[44]

Furthermore, the true value of using the oxide–halide perovskite upside-down composite method to potentially recycle piezoceramics comes when considering the energy budget of fabrication (designated as 'Φ' in Fig. 5b and Table 2). The Φ value was calculated based on the product of peak temperature and hold time implemented in each type of fabrication process to produce the desired functionality, as has been reported in previous work.[7] For instance, in the solid-state route, the product of calcination temperature and time and that of sintering temperature and time were summed to provide a measure of energy budget needed for producing a piezoceramic sample that could exhibit desired piezoelectric properties. This parameter, Φ, is assigned the unit $\times 10^3$ °C h.

It is obvious from Fig. 5b that, if sourcing the filler materials from waste piezoceramics, whilst being able to induce similar or larger g_{33}, the upside-down composite fabrication method enabled a considerably lower Φ value, which was only about 1% of that to be used for fabrication of new piezoceramics.

Therefore, both the lower Φ and larger g_{33} in S-PZT-C compared to its own piezoceramic counterpart as well as to other high-performance piezoceramics (Fig. 5b and Table 2) sufficiently demonstrated the feasibility of the oxide–halide upside-down composite and recyclability of piezoceramics *via* such a method. It is also noted that in addition to S-PZT-C, H-PZT-C also showed a comparable g_{33} ($\approx$22 mV m N^{-1}) to those of S-PZT-P and H-PZT-P but with a negligible Φ. This implies that deployed piezoceramics like S-PZT and H-PZT in aged/worn-out devices could be potentially recycled and be made for a second life in applications demanding high g_{33}, such as sensors, but at a much lower energy price. This would eventually contribute to sustainable production and use of toxic and hazardous Pb-based piezoelectric materials by avoiding, or at least postponing, the disposal of old PZT-based components that have a negative environmental contribution.

Recyclability using the oxide–halide perovskite upside-down composite method could also be proven with Pb-free piezoelectric compositions, with BT-C and KNBNNO-C showing g_{33}

Table 2 Summary of piezoelectric properties and energy budget of fabrication for Pb-free and Pb-based piezoelectric ceramics and composites which were fabricated in this work and selected from the literature

Sample ID/material	Densification method	Maximum processing temperature (°C)	g_{33} (mV m N^{-1})	FOM ($\times 10^{-12}$ m^2 N^{-1})	Φ ($\times 10^3$ °C h)	Reference
BT-P	Solid-state sintering	1450	26.7 ± 0.2	7.9 ± 0.1	10.2	This work
BT-C	Upside-down composite	150	19.2 ± 1.7	0.9 ± 0.2	0.1	This work
BT	Reactive hydrothermal liquid-phase densification	240	9.0[a]	0.8	17.3	53
BT	Sintering with LiF as sintering aid	1100	10.7[a]	2.9	6.6[b]	54
BCZT	Sol–gel followed by solid-state sintering	1450	29.0	18.5	5.7	55
BCZT	Sintering with CeO_2 as sintering aid	1350	14.0[a]	8.4	7.9	56
KNBNNO-P	Solid-state sintering	1150	11.7 ± 0.2	1.0 ± 0.0	5.3	This work
KNBNNO-C	Upside-down composite	150	12.9 ± 1.0	0.3 ± 0.0	0.1	This work
$(K_{0.5}Na_{0.5})NbO_3$	Cold sintering-assisted sintering	1115	19.7[a]	2.6	7.9	57
$(K_{0.5}Na_{0.5})NbO_3$	Solid-state sintering	1115	33.0[a]	3.9	7.9	57
$(K_{0.5}Na_{0.5})NbO_3$	Cold sintering followed by annealing	850	20.2	3.0	5.6	58
$0.98(K_{0.5}Na_{0.5})NbO_3$–$0.02Ba(Ni_{0.5}Nb_{0.5})O_{3-\Delta}$	Solid-state sintering	1165	11.9 ± 0.8	1.2 ± 0.2	5.7	32
$0.965(K_{0.48}Na_{0.52})(Nb_{0.95}Sb_{0.05})O_3$–$0.035Bi_{0.5}(Na_{0.82}K_{0.18})_{0.5}HfO_3$	Solid-state sintering	1090	23.7[a]	12.5	8.4	48
$0.96(K_{0.48}Na_{0.52})(Nb_{0.95}Sb_{0.05})O_3$–$0.04Bi_{0.5}(Na_{0.82}K_{0.18})_{0.5}ZrO_3$	Solid-state sintering	1085	25.2[a]	12.3	8.4	49
0.3 wt% ZnO-doped $(K_{0.5}Na_{0.5})NbO_3$–$0.02(Bi_{0.5}Li_{0.5})TiO_3$–$0.06BaZrO_3$	Sintering with ZnO as sintering aid	1200	18.2[a]	6.4	8.4	50
H-PZT-P	Solid-state sintering	1100	24.3 ± 0.2	4.8 ± 0.1	8.0[b]	This work
H-PZT-C	Upside-down composite	150	21.8 ± 0.9	0.9 ± 0.1	0.1	This work
S-PZT-P	Solid-state sintering	1200	24.3 ± 1.3	12.4 ± 1.4	6.0[b]	This work
S-PZT-C	Upside-down composite	150	36.0 ± 2.4	3.5 ± 0.5	0.1	This work
S-PZT–LMO	Upside-down composite	22	32.7	2.7	0.0	16
S-PZT-(am-TiO_2)	Upside-down composite	350	51.7	7.8	0.4[b]	17
PZT-5A	Cold sintering followed by annealing	900	16.8[a]	3.3	28.7	52
2.5 mol% Sm-doped 0.7PMN–0.3PT	Solid state sintering	1250	15.3[a]	16.7	11.9	51

[a] Details on whether measured permittivity was from an unpoled or poled sample were not provided in the reference for g_{33} calculation. [b] Details for calculation of Φ were not fully provided in the cited study and a close substitute was used instead.

values of ≈19 mV m N^{-1} and ≈13 mV m N^{-1}, respectively. Although these g_{33} values were not as competitive as those of their Pb-based counterparts, the significantly low Φ still provides an incentive to recycle Pb-free piezoceramics which had already offered potential environmental benefits by replacing Pb. On top of the environmental benefits, recycling Pb-free piezoceramics would offer additional benefits of saving on energy and material resource for our planet.

Table 2 also compares the piezoelectric energy harvesting figure of merit (FOM = $d_{33} \times g_{33}$), which is a universal indicator of energy conversion capability in kinetic energy harvesting applications.[3] A FOM value of ≈3.5 × 10^{-12} m^2 N^{-1} put the recycled sample, S-PZT-C, at the middle level among selected piezoceramics prepared *via* the solid-state high-temperature sintering route. However, if factors such as energy payback time,[7] scaling-up capability and integration compatibility with other low-temperature fabricated components are emphasized in practice, the upside-down composite method may make the moderate FOM still attractive in some lower-end energy harvesters that require cost-effectiveness which could tolerate the use of recycled materials with reduced FOM.

4. Critical outlook

In this work, commercial piezoelectric ceramics (purchased from Morgan Technical Ceramics Plc, UK), referred to as O.S-PZT-P, which were older than 20 years, were also truly recycled using the method reported above. Table 3 compares the properties of the O.S-PZT-P with those claimed by the manufacturer in freshly made samples as well as those of S-PZT-P, S-

Table 3 Summary of d_{33}, ε_r, and g_{33} of the S-PZT and O.S-PZT ceramics and upside-down composites

Material	d_{33} (pC N^{-1})	ε_r after poling at 1 kHz (—)	g_{33} (mV m N^{-1})	Reference
Soft-type PZT ceramic	630	3300[a]	21	38
S-PZT-P	509	2363	24	This work
O.S-PZT-P	588	2460	27	This work
S-PZT-C	97	304	36	This work
O.S-PZT-C	30	240	14	This work

[a] Information about poling and frequency was not given in the manufacturer's datasheet.

PZT-C, and O.S-PZT-C. The O.S-PZT-C sample was made *via* the following process: (1) removing the electrodes of O.S-PZT-P by sanding; (2) depoling at 500 °C; (3) crushing and sieving to obtain the filler and then making composites using the same method described in Section 2.

It can be noticed in Table 3 that by recycling O.S-PZT-P, the O.S-PZT-C only showed one third of the d_{33} and g_{33} values of S-PZT-C. However, such performance deterioration is not considered a disadvantage of the recycling method itself. This is because after two decades, the commercial piezoelectric material (O.S-PZT-P) aged by only 6–7%. Meanwhile, the S-PZT-C was also made with the same commercial calcined soft-type PZT powder that was the same two-decade old. This implies that the decreased properties shown by O.S-PZT-C should have been caused by factors which need further investigation. Even if recycling retired components would lead to the property decrease, there can still be freshly made but rejected materials during the manufacturing process that can be recycled using the method presented in this work. More importantly, the decreased g_{33} value obtained from O.S-PZT-C was still rather decent and was comparable to the manufacturer claimed value for freshly made ceramics. Considering the negligible energy consumption, the recycling method is still highly appealing for retired materials.

In addition to age, mechanical properties may also affect the performance of the recycled materials. In order to understand this aspect, impedance analysis was carried out with an impedance analyzer (E4990A, Keysight, USA) for $BaTiO_3$ ceramic and BT-C samples. Electromechanical and mechanical properties were then assessed *via* eqn (5)–(7),[24] where k_{eff} is the effective electromechanical coupling coefficient, Y_{11}^E is Young's modulus, Q_M is the mechanical quality factor, f_r is resonance frequency, f_a is anti-resonance frequency, ρ_m is the measured density of the material, d is sample diameter, $|Z_m|$ is impedance at resonance, and C_T is the sample's capacitance at 1 kHz. Table 4 compares the impedance analysis results.

$$k_{eff} \approx \frac{f_a^2 - f_r^2}{f_a^2} \quad (5)$$

Table 4 Comparison of the electromechanical and mechanical properties between $BaTiO_3$ ceramic and BT-C samples

Material	k_{eff}	Y_{11}^E (GPa)	Q_M (—)
$BaTiO_3$ ceramic	0.35	195	106
BT-C	0.23	54	21

$$Y_{11}^E = 4\rho_m(f_r^2)(d^2) \quad (6)$$

$$Q_M = \frac{1}{2\pi|Z_m|k_{eff}C_T f_r} \quad (7)$$

According to Table 4, the composite could achieve about 66% of the k_{eff} value of the ceramic counterparts, implying that the electromechanical coupling of the composite samples was still comparable to that of the ceramics. Due to the softness of the binder, the composite could only yield about 28% of the Young's modulus value, and about 20% of the mechanical quality factor value, of the ceramic counterparts. Such a decrease in mechanical properties may shorten the lifetime of the composites for heavy-load applications. For this reason, the recycled materials should be used with light duty, and further research should find ways to improve the mechanical properties of the composites.

With regards to the effect of possible material aging on the lifespan, the aging of the binder might be an issue. However, it is proven that stable d_{33} for at least one year can be achieved when utilizing 0.1 wt% of recycled $MAPbI_3$ as addition in the binder phase.[9] This was attributed to the suppression of the depolarization field present in the composite by the $MAPbI_3$ which has both high permittivity and conductivity. Therefore, material aging is not likely a concern for lifespan of the composites.

5. Conclusions

Upside-down composites consisting of an oxide perovskite filler and halide perovskite binder have been successfully fabricated. These newly made composites have demonstrated a potential recycling method for both Pb-based and Pb-free piezoceramics. No cross-reactions between the filler and binder have been observed from the microstructure, which is an expected consequence of the ultralow-temperature densification route. Dense packing between filler and binder particles with high filler volume fraction has been achieved.

The fabricated oxide–halide upside-down composites have exhibited lower relative permittivity, higher dielectric loss and lower piezoelectric charge coefficient compared to their ceramic counterparts due to a combined influence of (i) composite effect with applied electric field concentrating on the low-permittivity binder, (ii) piezoelectrically inactive binder, and (iii) porosity. The largest d_{33} value has been found in the soft-PZT composite

($\approx$100 pC N^{-1}) followed by the BT composite ($d_{33} \approx$ 45 pC N^{-1}), hard-PZT composite ($d_{33} \approx$ 40 pC N^{-1}), and KNBNNO composite ($d_{33} \approx$ 20 pC N^{-1}).

Despite the inferior piezoelectric charge coefficient, the fabricated composites have been competitive in terms of piezoelectric voltage coefficient with the soft-PZT composite showing the largest g_{33} value ($\approx$36 mV m N^{-1}) followed by the hard-PZT composite ($g_{33} \approx$ 22 mV m N^{-1}) and BT composite ($g_{33} \approx$ 19 mV m N^{-1}). This performance, derived from a more drastic decrease of permittivity than d_{33} from ceramic fillers to composites, is comparable to those of high-temperature sintered piezoceramics. More importantly, the energy budget needed to fabricate the oxide–halide perovskite upside-down composites from recycled filler materials is negligible compared to making new respective piezoceramics.

This provides a strong motivation for future recycling of piezoceramics from aged and retired piezoelectric devices *via* this method and then giving the recycled materials a second life in sensing applications. The moderate energy harvesting figure of merit obtained from soft-PZT composites may also be suitable for less-demanding energy harvesters made from recycled materials.

Prospective future works may include exploration of approaches for further increasing the piezoelectric charge coefficient using piezoceramic fillers with ultrahigh permittivity coupled with an ultrahigh piezoelectric charge coefficient. High permittivity may promote the composite effect, decrease overall permittivity of the composite, and thereby increase the piezoelectric voltage coefficient when subject to sufficient poling. Also, a higher piezoelectric charge coefficient directly contributes to a higher piezoelectric voltage coefficient in the composite. Families of BCZT and high-performance KNN piezoceramics[6] may be good filler candidates. Meanwhile, experimenting with a piezoelectrically active binder, seeking for non-toxic binders (*e.g.*, Cd-free options), and incorporating halide perovskites that are used in solar cells as binders may also be future research directions in order to further improve the generic piezoelectric properties of recycled materials, enhance the environmental friendliness of this recycling method, and reduce the carbon footprint of the energy and electronics industries, respectively.

Data availability

Data associated with this work are available at **https://doi.org/10.23729/099a0c0b-c416-45c2-832e-27c6bfa1ae15**.

Author contributions

S. S. A. – data curation, formal analysis, investigation, methodology, visualization, writing-original draft, writing-review & editing. M. T. – data curation, methodology. M. N. – investigation, methodology, supervision, writing review & editing. J. P. – investigation, supervision, writing-review & editing. H. J. – conceptualization, funding acquisition, resources. J. J. – funding acquisition, resources. Y. B. – conceptualization, formal analysis, funding acquisition, methodology, project administration, resources, supervision, validation, writing-review & editing.

Conflicts of interest

There are no conflicts to declare.

Acknowledgements

This research has been funded by Infotech Institute, University of Oulu as a spearhead project. The authors acknowledge the Centre for Material Analysis, University of Oulu for providing necessary equipment and facilities. The authors also acknowledge Dr Jaakko Palosaari and Mr Vasilii Balanov for research assistance.

References

1 A. J. Moulson and J. M. Herbert, *Electroceramics: Materials, Properties, Applications*, Wiley, West Sussex, 2003, pp. 1–4, 103–114, 114–118, 361, 387–402.
2 K. Uchino, *Introduction to Piezoelectric Actuators and Transducers*, Int. Cent. Actuators Transducers, Penn State Univ., 2003, vol. 40.
3 Y. Bai, H. Jantunen and J. Juuti, Energy harvesting research: the road from single source to multisource, *Adv. Mater.*, 2018, **30**(34), 1707271, DOI: **10.1002/adma.201707271**.
4 J. Rödel, K. G. Webber, R. Dittmer, W. Jo, M. Kimura and D. Damjanovic, Transferring lead-free piezoelectric ceramics into application, *J. Eur. Ceram. Soc.*, 2015, **35**(6), 1659–1681, DOI: **10.1016/j.jeurceramsoc.2014.12.013**.
5 J. Rödel, W. Jo, K. T. P. Seifert, E. M. Anton, T. Granzow and D. Damjanovic, Perspective on the development of lead-free piezoceramics, *J. Am. Ceram. Soc.*, 2009, **92**(6), 1153–1177, DOI: **10.1111/j.1551-2916.2009.03061.x**.
6 T. Zheng, J. Wu, D. Xiao and J. Zhu, Recent development in lead-free perovskite piezoelectric bulk materials, *Prog. Mater. Sci.*, 2018, **98**, 552–624, DOI: **10.1016/j.pmatsci.2018.06.002**.
7 S. S. Anandakrishnan, S. Yadav, M. Tabeshfar, *et al.*, Toward Ecofriendly Piezoelectric Ceramics—Reduction of Energy and Environmental Footprint from Conceptualization to Deployment, *Global Challenges*, 2023, 2300061, DOI: **10.1002/gch2.202300061**.
8 J. Guo, R. Floyd, S. Lowum, *et al.*, Cold Sintering: Progress, Challenges, and Future Opportunities, *Annu. Rev. Mater. Res.*, 2019, **49**, 275–295, DOI: **10.1146/annurev-matsci-070218-010041**.
9 M. Tabeshfar, M. Nelo, S. S. Anandakrishnan, M. Siddiqui, J. Peräntie, P. Tofel, H. Jantunen, J. Juuti and Y. Bai, Oxide-halide perovskite composites for simultaneous recycling of lead zirconate titanate piezoceramics and methylammonium lead iodide solar cells, *Small Methods*, 2023, 2300830.
10 H. Kähäri, M. Teirikangas, J. Juuti and H. Jantunen, Dielectric Properties of Lithium Molybdate Ceramic Fabricated at Room Temperature, *J. Am. Ceram. Soc.*, 2014, **97**(11), 3378–3379, DOI: **10.1111/jace.13277**.

11 H. Kähäri, M. Teirikangas, J. Juuti and H. Jantunen, Improvements and modifications to room-temperature fabrication method for dielectric Li_2MoO_4 ceramics, *J. Am. Ceram. Soc.*, 2015, **98**(3), 687–689, DOI: 10.1111/jace.13471.
12 H. Kähäri, M. Teirikangas, J. Juuti and H. Jantunen, Room-temperature fabrication of microwave dielectric Li_2MoO_4-TiO_2 composite ceramics, *Ceram. Int.*, 2016, **42**(9), 11442–11446, DOI: 10.1016/j.ceramint.2016.04.081.
13 H. Guo, A. Baker, J. Guo and C. A. Randall, Protocol for Ultralow-Temperature Ceramic Sintering: An Integration of Nanotechnology and the Cold Sintering Process, *ACS Nano*, 2016, **10**(11), 10606–10614, DOI: 10.1021/acsnano.6b03800.
14 N. Kuzmić, S. D. Škapin, M. Nelo, H. Jantunen and M. Spreitzer, Dielectric Properties of Upside-Down $SrTiO_3$/Li_2MoO_4 Composites Fabricated at Room Temperature, *Front. Mater.*, 2021, **8**, 669421, DOI: 10.3389/fmats.2021.669421.
15 M. Nelo, J. Peräntie, T. Siponkoski, J. Juuti and H. Jantunen, Upside-down composites: electroceramics without sintering, *Appl. Mater. Today*, 2019, **15**, 83–86, DOI: 10.1016/j.apmt.2018.12.021.
16 M. Nelo, T. Siponkoski, H. Kähäri, K. Kordas, J. Juuti and H. Jantunen, Upside - down composites: fabricating piezoceramics at room temperature, *J. Eur. Ceram. Soc.*, 2019, **39**(11), 3301–3306, DOI: 10.1016/j.jeurceramsoc.2019.04.052.
17 T. Siponkoski, M. Nelo, N. Ilonen, J. Juuti and H. Jantunen, High performance piezoelectric composite fabricated at ultra low temperature, *Composites, Part B*, 2022, **229**, 109486, DOI: 10.1016/j.compositesb.2021.109486.
18 Y. Hu, L. You, B. Xu, *et al.*, Ferroelastic-switching-driven large shear strain and piezoelectricity in a hybrid ferroelectric, *Nat. Mater.*, 2021, **20**(5), 612–617, DOI: 10.1038/s41563-020-00875-3.
19 N. Ma, B. P. Zhang, W. G. Yang and D. Guo, Phase structure and nano-domain in high performance of $BaTiO_3$ piezoelectric ceramics, *J. Eur. Ceram. Soc.*, 2012, **32**(5), 1059–1066, DOI: 10.1016/j.jeurceramsoc.2011.11.014.
20 Y. Bai, A. A. Kistanov, W. Cao and J. Juuti, Vacancy-Induced Niobate Perovskite-Tungsten Bronze Composite for Synergetic Tuning of Ferroelectricity and Band Gaps, *J. Phys. Chem. C*, 2021, **125**(16), 8890–8898, DOI: 10.1021/acs.jpcc.1c01845.
21 H. Zheng, I. M. Reaney, W. E. Lee, N. Jones and H. Thomas, Effects of octahedral tilting on the piezoelectric properties of strontium/barium/niobium-doped soft lead zirconate titanate ceramics, *J. Am. Ceram. Soc.*, 2004, **85**(9), 2337–2344, DOI: 10.1111/j.1151-2916.2002.tb00457.x.
22 M. Algueró, F. Guiu and M. J. Reece, Degradation of PZT-4D hard piezoceramics under moderate heating, *J. Eur. Ceram. Soc.*, 2000, **20**(16), 2705–2711, DOI: 10.1016/S0955-2219(00)00221-1.
23 H. Birol, D. Damjanovic and N. Setter, Preparation and characterization of $KNbO_3$ ceramics, *J. Am. Ceram. Soc.*, 2005, **88**(7), 1754–1759, DOI: 10.1111/j.1551-2916.2005.00347.x.
24 Y. Bai, Vibrational Energy Harvesting Using Piezoelectric Ceramics and Free-Standing Thick-Film Structures, PhD thesis, University of Birmingham, 2015.
25 S. S. Anandakrishnan, *Data of Recycling Hazardous and Energy-Demanding Piezoelectric Ceramics Using the Oxide-Halide Perovskite Upside-Down Composite Method*, 2024, DOI: 10.23729/099a0c0b-c416-45c2-832e-27c6bfa1ae15.
26 M. Acosta, N. Novak, V. Rojas, *et al.*, $BaTiO_3$-based piezoelectrics: fundamentals, current status, and perspectives, *Appl. Phys. Rev.*, 2017, **4**(4), 041305, DOI: 10.1063/1.4990046.
27 J. Gao, D. Xue, W. Liu, C. Zhou and X. Ren, Recent progress on $BaTiO_3$-based piezoelectric ceramics for actuator applications, *Actuators*, 2017, **6**(3), 24, DOI: 10.3390/act6030024.
28 Samsung-Electro-Mechanics, *MLCC – Multilayer Ceramic Capacitors*, Samsung-Electro-Mechanics, https://www.samsungsem.com/global/product/passive-component/mlcc.do, accessed on August 17, 2023.
29 Y. Bai, H. Xiang, H. Jantunen and J. Juuti, Multi-functional perovskites – an investigation of compositional and processing influence on microstructure, dielectric and ferroelectric properties, *Eur. Phys. J.: Spec. Top.*, 2019, **228**, 1555–1573, DOI: 10.1140/epjst/e2019-800132-8.
30 Y. Bai, H. Jantunen and J. Juuti, Ferroelectric Oxides for Solar Energy Conversion, Multi-Source Energy Harvesting/Sensing, and Opto-Ferroelectric Applications, *ChemSusChem*, 2019, **12**(12), 2540–2549, DOI: 10.1002/cssc.201900671.
31 Y. Bai, Z. Havránek, P. Tofel, C. Meggs, H. Hughes and T. W. Button, Nonlinear piezoelectric devices for broadband air-flow energy harvesting, *Eur. Phys. J.: Spec. Top.*, 2015, **224**, 2675–2685, DOI: 10.1140/epjst/e2015-02582-8.
32 Y. Bai, J. Palosaari, P. Tofel and J. Juuti, A Single-Material Multi-Source Energy Harvester, Multifunctional Sensor, and Integrated Harvester—Sensor System—Demonstration of Concept, *Energy Technol.*, 2020, **8**(9), 2000461, DOI: 10.1002/ente.202000461.
33 Z. Yu, C. Ang, R. Guo and A. S. Bhalla, Piezoelectric and strain properties of $Ba(Ti_{1-x}Zr_x)O_3$ ceramics, *J. Appl. Phys.*, 2002, **92**(3), 1489–1493, DOI: 10.1063/1.1487435.
34 Y. Bai, P. Tofel, J. Palosaari, H. Jantunen and J. Juuti, A Game Changer: A Multifunctional Perovskite Exhibiting Giant Ferroelectricity and Narrow Bandgap with Potential Application in a Truly Monolithic Multienergy Harvester or Sensor, *Adv. Mater.*, 2017, **29**(29), 1700767, DOI: 10.1002/adma.201700767.
35 K. Uchino, J. Zheng, A. Joshi, *et al.*, High Power Characterization of Piezoelectric Materials, *J. Electroceram.*, 1998, **2**(1), 33–40, DOI: 10.1023/A:1009962925948.
36 V. Kovaľ and J. Briančin, Effect of poling process on the piezoelectric and dielectric properties of Nb and Sr-doped PZT ceramics, *Ferroelectrics*, 1997, **193**(1–4), 41–49, DOI: 10.1080/00150199708228319.
37 A. K. Arora, R. P. Tandon and A. Mansingh, Piezoelectric, pyroelectric and dielectric properties of lanthanum

modified lead zirconate titanate ceramics, *Ferroelectrics*, 1992, **132**(1), 9–25.

38 Americanpiezo International Ltd, *Physical and Piezoelectric Properties of APC Materials*, Am Int. Ltd., https://www.americanpiezo.com/apc-materials/piezoelectric-properties.html, accessed on August 17, 2023.

39 Ferroperm Piezoceramics, *Soft PZT type Pz29 data sheet*, Ferroperm Piezoceramics, https://www.ferropermpiezoceramics.com/wp-content/uploads/2021/10/Datasheet-soft-pz29.pdf, accessed on August 17, 2023.

40 R. Guo, J. I. Roscow, C. R. Bowen, *et al.*, Significantly enhanced permittivity and energy density in dielectric composites with aligned $BaTiO_3$ lamellar structures, *J. Mater. Chem. A*, 2020, **8**, 3135–3144, DOI: 10.1039/c9ta11360f.

41 Prateek, V. K. Thakur and R. K. Gupta, Recent Progress on Ferroelectric Polymer-Based Nanocomposites for High Energy Density Capacitors: Synthesis, Dielectric Properties, and Future Aspects, *Chem. Rev.*, 2016, **116**(7), 4260–4317, DOI: 10.1021/acs.chemrev.5b00495.

42 N. Jayasundere, B. V. Smith and J. R. Dunn, Piezoelectric constant for binary piezoelectric 0-3 connectivity composites and the effect of mixed connectivity, *J. Appl. Phys.*, 1994, **76**(5), 2993–2998, DOI: 10.1063/1.357546.

43 H. Luo, J. Roscow, X. Zhou, *et al.*, Ultra-high discharged energy density capacitor using high aspect ratio $Na_{0.5}Bi_{0.5}TiO_3$ nanofibers, *J. Mater. Chem. A*, 2017, **5**(15), 7091–7102, DOI: 10.1039/c7ta00136c.

44 Y. Zhang, M. Xie, J. Roscow, *et al.*, Enhanced pyroelectric and piezoelectric properties of PZT with aligned porosity for energy harvesting applications, *J. Mater. Chem. A*, 2017, **5**(14), 6569–6580, DOI: 10.1039/c7ta00967d.

45 J. Khaliq, D. B. Deutz, J. A. C. Frescas, *et al.*, Effect of the piezoelectric ceramic filler dielectric constant on the piezoelectric properties of PZT-epoxy composites, *Ceram. Int.*, 2017, **43**(2), 2774–2779, DOI: 10.1016/j.ceramint.2016.11.108.

46 X. Yan, M. Zheng, M. Zhu and Y. Hou, Soft and hard piezoelectric ceramics for vibration energy harvesting, *Crystals*, 2020, **10**, 907, DOI: 10.3390/cryst10100907.

47 J. Holterman and P. Groen, *An Introduction to Piezoelectric Materials and Applications*, Stichting Applied Piezo, Apeldoorn, 2013, pp. 87–89.

48 T. Zheng, H. Wu, Y. Yuan, *et al.*, The structural origin of enhanced piezoelectric performance and stability in lead free ceramics, *Energy Environ. Sci.*, 2017, **10**(2), 528–537, DOI: 10.1039/c6ee03597c.

49 T. Zheng, J. Wu, D. Xiao, J. Zhu, X. Wang and X. Lou, Potassium-sodium niobate lead-free ceramics: modified strain as well as piezoelectricity, *J. Mater. Chem. A*, 2015, **3**(5), 1868–1874, DOI: 10.1039/c4ta05423g.

50 J. W. Li, Y. X. Liu, H. C. Thong, *et al.*, Effect of ZnO doping on $(K,Na)NbO_3$-based lead-free piezoceramics: enhanced ferroelectric and piezoelectric performance, *J. Alloys Compd.*, 2020, **847**, 155936, DOI: 10.1016/j.jallcom.2020.155936.

51 Y. Yang, E. Sun, Z. Xu, *et al.*, Sm and Mn co-doped PMN-PT piezoelectric ceramics: defect engineering strategy to achieve large d_{33} and high Qm, *J. Mater. Sci. Technol.*, 2023, **137**, 143–151, DOI: 10.1016/j.jmst.2022.08.004.

52 D. Wang, H. Guo, C. S. Morandi, C. A. Randall and S. Trolier-McKinstry, Cold sintering and electrical characterization of lead zirconate titanate piezoelectric ceramics, *APL Mater.*, 2018, **6**, 016101, DOI: 10.1063/1.5004420.

53 L. Karacasulu, M. Tokkan, M. Bortolotti, G. Ischia, U. Adem and C. Vakifahmetoglu, Electrical characteristics of low temperature densified barium titanate, *Ceram. Int.*, 2020, **46**(10), 16670–16676, DOI: 10.1016/j.ceramint.2020.03.240.

54 W. G. Yang, B. P. Zhang, N. Ma and L. Zhao, High piezoelectric properties of $BaTiO_{3-x}LiF$ ceramics sintered at low temperatures, *J. Eur. Ceram. Soc.*, 2012, **32**(4), 899–904, DOI: 10.1016/j.jeurceramsoc.2011.10.054.

55 J. P. Praveen, T. Karthik, A. R. James, E. Chandrakala, S. Asthana and D. Das, Effect of poling process on piezoelectric properties of sol-gel derived BZT-BCT ceramics, *J. Eur. Ceram. Soc.*, 2015, **35**(6), 1785–1798, DOI: 10.1016/j.jeurceramsoc.2014.12.010.

56 Y. Cui, X. Liu, M. Jiang, *et al.*, Lead-free $(Ba_{0.85}Ca_{0.15})(Ti_{0.9}Zr_{0.1})O_3$-$CeO_2$ ceramics with high piezoelectric coefficient obtained by low-temperature sintering, *Ceram. Int.*, 2012, **38**(6), 4761–4764, DOI: 10.1016/j.ceramint.2012.02.063.

57 J. Ma, H. Li, H. Wang, *et al.*, Composition, microstructure and electrical properties of $K_{0.5}Na_{0.5}NbO_3$ ceramics fabricated by cold sintering assisted sintering, *J. Eur. Ceram. Soc.*, 2019, **39**(4), 986–993, DOI: 10.1016/j.jeurceramsoc.2018.11.044.

58 B. Deng, Y. Ma, T. Chen, *et al.*, Elevating electrical properties of $(K, Na)NbO_3$ ceramics *via* cold sintering process and post-annealing, *J. Am. Ceram. Soc.*, 2022, **105**(1), 461–468, DOI: 10.1111/jace.18103.

59 D. A. Van Den Ende, B. F. Bory, W. A. Groen and S. Van Der Zwaag, Improving the d_{33} and g_{33} properties of 0-3 piezoelectric composites by dielectrophoresis, *J. Appl. Phys.*, 2010, **107**, 024107, DOI: 10.1063/1.3291131.